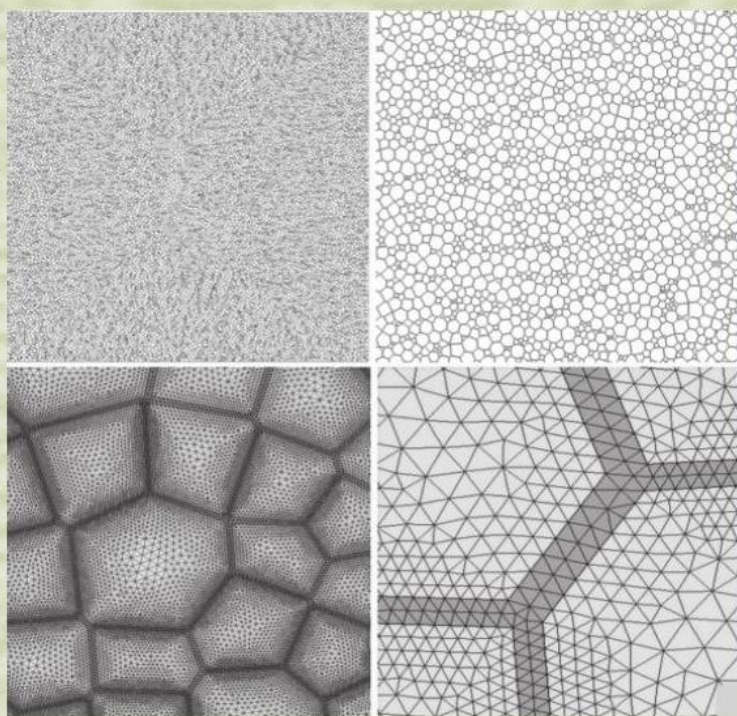


# Advanced Materials Science and Technology



Edited by  
Jian Lu

# **Advanced Materials Science and Technology**

# **Advanced Materials Science and Technology**

Selected, peer reviewed papers from the 6th International Forum on  
Advanced Material Science and Technology (IFAMST 2008),  
12-14 June 2008, The Hong Kong Polytechnic University, Hong Kong SAR,  
China

*Edited by:*

**Jian Lu**

The Hong Kong Polytechnic University  
Hong Kong SAR, China

 **TRANS TECH PUBLICATIONS LTD**  
**Switzerland • UK • USA**

**Copyright** © 2009 Trans Tech Publications Ltd, Switzerland

All rights reserved. No part of the contents of this publication may be reproduced or transmitted in any form or by any means without the written permission of the publisher.

Trans Tech Publications Ltd  
Laubisrutistr. 24  
CH-8712 Stafa-Zurich  
Switzerland  
<http://www.ttp.net>

Volume 614 of  
*Materials Science Forum*  
ISSN 0255-5476

Full text available online at <http://www.scientific.net>

***Distributed*** worldwide by

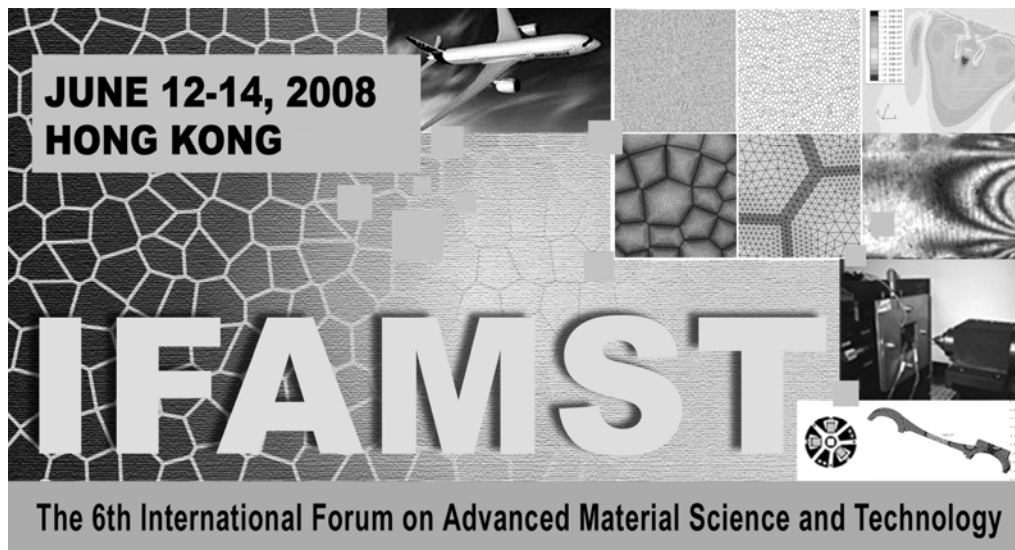
Trans Tech Publications Ltd  
Laubisrutistr. 24  
CH-8712 Stafa-Zurich  
Switzerland

Fax: +41 (44) 922 10 33  
e-mail: [sales@ttp.net](mailto:sales@ttp.net)

and in the Americas by

Trans Tech Publications Inc.  
PO Box 699, May Street  
Enfield, NH 03748  
USA

Phone: +1 (603) 632-7377  
Fax: +1 (603) 632-5611  
e-mail: [sales-usa@ttp.net](mailto:sales-usa@ttp.net)



The 6<sup>th</sup> International Forum on  
Advanced Material Science and Technology  
(IFAMST 2008)

12-14 June 2008  
The Hong Kong Polytechnic University  
Hong Kong SAR, China

Organized by  
The Hong Kong Polytechnic University

Sponsored by  
Saitama Institute of Technology  
The Hong Kong Polytechnic University  
Hong Kong Society of Theoretical and Applied Mechanics

## **International Scientific Advisory Committee**

Prof. T. Ericsson	Linköping University, Sweden
Prof. D. N. Fang	Tsinghua University, China
Prof. T. N. Farris	Purdue University, USA
Prof. Q. C. He	Universite de Marne-la-Valee, France
Prof. J.T.M. De Hosson	University of Groningen, The Netherlands
Prof. T. Inoue	Fukuyama University, Japan
Prof. V. Ji	Universite Paris-Sud 11, France
Prof. Y. Y. Li	Institute of Metal Research, China
Dr. Z. Li	Brookhaven National Laboratory, USA
Dr. C. T. Liu	Oak Ridge National Laboratory, USA
Prof. K. Lu	Chinese Academy of Science, China
Prof. Y. W. Mai	The University of Sydney, Australia
Prof. C. Nan	Tsinghua University, China
Dr. S. Nemat-Nasser	University of California, USA
Prof. S. Phillpot	University of Florida, USA
Prof. R. O. Ritchie	University of California, Berkeley, USA
Prof. B. Scholtes	Uniersität Gesamthochschule Kassel, Germany
Dr. R. D. Shull	National Institute of Standards & Technology, USA
Prof. K. Tanaka	Saitama Institute of Technology, Japan
Prof. Z. L. Wang	Georgia Institute of Technology, USA
Prof. G. J. Weng	Rutgers University, USA
Prof. C. P. Wong	Georgia Institute of Technology, USA
Prof. J. X. Xie	University of Science and Technology Beijing, China
Prof. W. Yang	Tsinghua University, USA
Prof. Q. M. Zhang	Penn State University, USA
Prof. S. J. Zhu	Fukuoka Institute of Technology, Japan
Prof. L. Zuo	Northeastern University, China

## **International Organizing Committee**

Prof. Jian Lu (Chairman)	The Hong Kong Polytechnic University, China
Prof. D.Y. Ju (Vice Chairman)	Saitama Institute of Technology, Japan
Prof. Y.C. Zhou (Vice Chairman)	Xiangtan University, China
Prof. H. M. Cheng	Institute of Metal Research, China
Dr. H. S. Dong	University of Birmingham, UK
Prof. A. Ivankovic	University College Dublin, Ireland
Prof. Y. Ju	Nagoya University, Japan
Prof. J. S. Leng	Harbin Institute of Technology, China
Prof. X. J. Liu	Xiamen University, China
Dr. S. H. J. Lo	Metals Technology Laboratories, Canada
Prof. Y. F. Lu	University of Nebraska-Lincoln, US
Prof. E. Ma	John Hopkins University, USA
Prof. Q. Q. Ni	Sinsyu University, Japan
Prof. J. M. Qu	Georgia Institute of Technology, USA
Prof. R. M. Ren	Dalian Jiaotong University, China
Prof. Y. Tan	Dalian University of Technology, China
Prof. Y. G. Wei	Institute of Mechanics, China
Dr. P. Xin	Covalent Materials Corporation, Japan
Dr. F. X. Yin	National Institute for Material Science, China
Prof. C. M. Zhang	University of Science and Technology, China

Prof. D. Zhang  
Prof. Y. Zhou

Shanghai Jiao Tong University, China  
Harbin Institute of Technology, China

**Local Organizing Committee**

Prof. Jian Lu (Chairman)	The Hong Kong Polytechnic University, HKSAR, China
Dr. M. W. Fu	The Hong Kong Polytechnic University, HKSAR, China
Dr. K. T. Lau	The Hong Kong Polytechnic University, HKSAR, China
Dr. S. W. R. Lee	The Hong Kong University of Science and Technology, HKSAR, China
Dr. Y. G. Shen	City University of Hong Kong, HKSAR, China
Prof. S. Q. Shi	The Hong Kong Polytechnic University, HKSAR, China
Prof. A. K. Soh	The University of Hong Kong, HKSAR, China
Prof. Q. P. Sun	The Hong Kong University of Science and Technology, HKSAR, China
Dr. Y. Yang	The Hong Kong Polytechnic University, HKSAR, China
Prof. T. Y. Zhang	The Hong Kong University of Science and Technology, HKSAR, China
Prof. L. M. Zhou	The Hong Kong Polytechnic University, HKSAR, China

## Editor's Preface

This volume contains 44 six-page full length papers presented at the 6<sup>th</sup> International Forum on Advanced Material Science and Technology (IFAMST 2008) held in The Hong Kong Polytechnic University, Hong Kong, China from 12 to 14 June 2008.

The full length papers of 6 invited papers are included in the beginning of the book. The remaining 38 full length papers are selected and arranged in 6 special sessions.

Started in 1998, the International Forum on Advanced Material Science and Technology (IFAMST) takes place every two years around the world. The previous five forums were successfully held in London of UK, Tokyo of Japan, Anshan of China, Troyes of France and Zhangjiajie of China. This is the first time that the international forum is hosted in Hong Kong. Its scope is to bring scientists and engineers of different countries working in various fields together for discussing about the latest development and world-wide cooperation concerned with advanced material science and technology. IFAMST 2008 was organized by The Hong Kong Polytechnic University and was sponsored by Saitama Institute of Technology, The Hong Kong Polytechnic University, Hong Kong Society of Theoretical and Applied Mechanics. IFAMST 2008 focused on all aspects of material science and technology with emphasis to nanostructured materials and nanostructures. The technical program of IFAMST 2008 was the product of hard work and devotion of more than 20 world leading experts to whom I am greatly indebted. The success of IFAMST 2008 relied solely on the dedication and titanic work of the members of Local Organizing Committee, the pillars of IFAMST 2008. As chairman of IFAMST 2008, I am honoured to have them on the Committee and have worked closely with them for a successful conference.

More than one hundred participants attended IFAMST 2008, while more than 80 papers were presented. The participants of IFAMST 2008 came from 11 countries. Roughly speaking, 50% of them were from Asia, 10% from Europe, 10% from America and 10% from other countries. I am happy and proud to have welcomed in Hong Kong well-known experts who came to discuss problems related to the analysis of advanced material science and technology.

I very sincerely thank the authors who have contributed to this volume and the referees who reviewed the quality of the submitted contributions. Our sponsors' support, either financial or moral, is gratefully acknowledged. The members of the Organizing Committee as well as other numerous individuals behind the scenes, especially Miss Joanne Cheng who acted as the Conference Secretary, are greatly appreciated for their tireless effort and dedication in the organization of the conference. Finally, a special word of thanks goes to Mr. Thomas Wohlbier and Ms. Anne Wohlbier of Trans Tech Publications Ltd. for the nice appearance of this book and his kind and continuous collaboration and support.

Jian Lu  
Chairman of IFASMT 2008  
The Hong Kong Polytechnic University  
Hong Kong, China

# Table of Contents

## Organizers

## Preface

## I. Invited Papers

<b>Formation of Metallic Micro/Nanomaterials by Utilizing Migration Phenomena and Techniques for their Applications</b> M. Saka, H. Tohmyoh, M. Muraoka, Y. Ju and K. Sasagawa	3
<b>Transformation Plasticity - The Mechanism and Some Applications</b> T. Inoue	11
<b>Nano-Size Surface Materials Stabilized by Weak Interaction</b> K. Tanaka and X.H. Jiang	21
<b>Advanced Numerical Simulation of Metal Forming Processes Using Adaptive Remeshing Procedure</b> A. Cherouat, L. Giraud-Moreau and H. Borouchaki	27
<b>Poroelectricity of Fluid-Saturated Nanoporous Media</b> V. Pensée, Q.C. He and H. Le Quang	35
<b>Experimental Evaluation of the Size Effect on the Ductile and Brittle Fracture Toughness of a Steel Pressure Vessel</b> Z.X. Wang, H.J. Shi and J. Lu	41

## II. Advanced Materials

<b>Synthesis and Properties of an Ultrafine Grained Ti-45Al-2Cr-2Nb-1B-0.5Ta Alloy Prepared by Double Mechanical Milling and Spark Plasma Sintering</b> Y.Y. Chen, F.T. Kong, H.B. Yu and D.L. Zhang	49
<b>The Effect of Heat Treatment on the Microstructure of Ti-45Al-5Nb-0.3Y Alloy</b> F.T. Kong and Y.Y. Chen	55
<b>Residual Stress Gradient Study of Laser Shocked Aluminum Alloy by GIXRD Analysis and FEM Simulation</b> H.B. Song, P. Peyre, V. Ji and H. Pelletier	61
<b>Bioactivating the Surfaces of Titanium by Sol-Gel Process</b> Y.C. Li, J.Y. Xiong, C.S. Wong, P.D. Hodgson and C.E. Wen	67
<b>Porous Ti/HA Biocomposites for Biomaterial Applications</b> Z.G. Liu, Y.M. Zhang, H. Shi, L.J. Xu, Y.Y. Chen and K.D. Woo	73
<b>Amperometric Biosensors Equipped with Enzyme Micelle Membrane Using Polymaleimido-styrene as Stabilizer</b> X.Y. Wang and S. Uchiyama	79
<b>Apatite Formation on Nano-Structured Titanium and Niobium Surface</b> X.J. Wang, J.Y. Xiong, Y.C. Li, P.D. Hodgson and C.E. Wen	85
<b>Evaluation of the Electromagnetic Characteristics on Ag/NiCuZn Ferrite Sintered Bodies</b> D.Y. Ju, P. Bian, H. Hou and Y.H. Zhao	93

## III. Material Processing

<b>Analysis of Metals Surface Structure Modifications Induced by High Current Pulsed Electron Beam (HCPEB) under the “Heating” and “Melting” Modes</b> T. Grosdidier, J.X. Zou, J. Wu, X.D. Zhang, K.M. Zhang, A.M. Wu, S.Z. Hao and C. Dong	99
<b>Production of Small Pin by Micro/Meso-Scale Rotary Forming</b> H.L. Zhang, T. Makino, K. Dohda and J. Cao	105
<b>Quantitative Evaluation of Wall Thinning of Metal Pipes by Microwaves</b> Y. Lu, L.S. Liu and M. Ishikawa	111

<b>Analysis on Process and Forming Defects of Large-Scale Complex Integral Component Isothermal Local Loading</b> Z.C. Sun and H. Yang	117
<b>Effects of Downstream Rolling on Microstructure and Mechanical Properties of Twin Roll Casting AZ31B Strip</b> H.Y. Zhao, X.D. Hu and D.Y. Ju	123
<b>Experimental and Numerical Studies of Welded Tubes Formability</b> A. Ayadi, A. Cherouat, M.A. Rezgui and N. Mezghani	129

#### IV. Mechanical Behavior of Material

<b>A Method for Improving Compressive Residual Stress of Small Holes Surface by Water-Jet Cavitation Peening</b> B. Han and D.Y. Ju	137
<b>Thermal Mechanical Behaviors and Microstructure Characteristics in Twin-Roll-Casting Process of Magnesium Alloy AZ31</b> X.D. Hu, H.Y. Zhao and D.Y. Ju	143
<b>Inside Residual Stress Analysis of Carburizing-Nitriding Quenching Spur Gear by Neutron Diffraction Method</b> R. Mukai, D.Y. Ju and H. Suzuki	149
<b>Strain Rate Evolution in Aluminium Alloy Measured by ESPI during Tensile Test</b> J. Petit, G. Montay and M. François	155
<b>Shot Peening Using Wet Blasting Machine with a Wide Nozzle</b> S. Sakoda and K. Tosha	163
<b>Visualization of Stress Distribution Using Smart Mechanoluminescence Sensor</b> W.X. Wang, T. Matsubara, Y. Takao, Y. Imai and C.N. Xu	169
<b>Snoek Relaxation in bcc Metals and High Damping <math>\beta</math>-Ti Alloys</b> F.X. Yin, L.M. Yu, D.H. Ping and S. Iwasaki	175
<b>Abrupt Softening Phenomenon in a Shape Memory CuAlNi Single Crystal under Uniaxial Compression</b> L. Sun and W.M. Huang	181

#### V. Nanomaterials

<b>Comparison of Surface Nanostructured Electrodeposited Cu Produced from Different Power Types: Microstructure and Tensile Properties</b> H.L. Chan and J. Lu	189
<b>Influence of Nanoparticles Modification on the Properties of Bitumen</b> S.P. Wu, G. Liu, J.G. Wang and Y. Zhang	197
<b>Nanostructured 316 Stainless Steel Prepared under Traction by Surface Mechanical Attrition Treatment</b> X.F. Yang and J. Lu	201
<b>Characterization of Radiation Hard Silicon Materials</b> P. Luukka, J. Härkönen, E. Tuovinen, S. Czellar, V. Eremin, Z. Li, E. Tuominen and E. Verbitskaya	207
<b>Radiation Hard Silicon for Medical, Space and High Energy Physics Applications</b> J. Härkönen, E. Tuovinen, P. Luukka, E. Tuominen, Z. Li, V. Eremin and E. Verbitskaya	215
<b>Effect of Additional Element and Heat Treating Temperature on the Microstructure and Mechanical Behaviour of Ag Thin Film</b> D.Y. Ju, S. Ishiguro, K. Hasegawa and T. Arizono	223
<b>Fabrication of Magnetite Nanoparticles and Drug Delivery Observation of Hydrophobe Ferrofluid by SPring-8 Synchrotron Radiation</b> D.Y. Ju, P. Bian, M. Nakano, H. Matsuura, K. Makino, N. Noda, K. Koide and T. Nemoto	229

#### VI. Polymer and Composite Materials

---

<b>Preparation and Electrochemical Capacitance of Ruthenium Oxide-Titania Nanotube Composite</b>	
Y.B. Xie, L.M. Zhou, C.J. Huang, Y. Liu and J. Lu	235
<b>Formation of Protrusive Micro/Nano Patterns atop Shape Memory Polymers</b>	
W.M. Huang, N. Liu, X. Lan, J.Q. Lin, J.H. Pan, J.S. Leng, S.J. Phee, H. Fan, Y.J. Liu and T.H. Tong	243
<b>High Strength Nanocrystallized Multilayered Structure Obtained by SMAT and Co-Rolling</b>	
L. Waltz, D. Retraint, A. Roos, P. Olier and J. Lu	249
<b>A Versatile Micromechanical Model for Estimating the Effective Properties of Isotropic Composite Materials</b>	
Q.C. He and H. Le Quang	255

## VII. Construction Materials

<b>The Experimental Research of a Heavyweight High-Strength Concrete</b>	
Y.S. Luo, H. Wang, W.B. Liu, S.C. Deng and Y.R. Ma	263
<b>Material Selection and Design for Moisture Damage of HMA Pavement</b>	
J.F. Huang, S.P. Wu, L.X. Ma and Z.F. Liu	269
<b>Nonlinear Stability Analysis on the Concrete Casting Step of Long-Span Concrete-Filled Steel Tube Arch Bridge</b>	
J. Wang, M.Z. Zhang and X.L. Guo	275
<b>Performances Research of Hybrid Fiber Reinforced Asphalt Concrete</b>	
S.P. Wu, H.B. Yue, Q.S. Ye and L. Pang	283
<b>Study on the Fatigue Property for Aged Asphalt Mixtures by Using Four Point Bending Tests</b>	
G.J. Zhu, S.P. Wu, R. Liu and L. Zhou	289

# **1. Invited Papers**

## Formation of Metallic Micro/Nanomaterials by Utilizing Migration Phenomena and Techniques for Their Applications

M. Saka<sup>1,a</sup>, H. Tohmyoh<sup>1,b</sup>, M. Muraoka<sup>2,c</sup>, Y. Ju<sup>3,d</sup> and K. Sasagawa<sup>4,e</sup>

<sup>1</sup>Department of Nanomechanics, Tohoku University, Sendai, JAPAN

<sup>2</sup>Department of Mechanical Engineering, Akita University, Akita, JAPAN

<sup>3</sup>Department of Mechanical Science and Engineering, Nagoya University, Nagoya, JAPAN

<sup>4</sup>Department of Intelligent Mechanics and System Engineering, Hirosaki University, Hirosaki, JAPAN

<sup>a</sup>saka@ism.mech.tohoku.ac.jp, <sup>b</sup>tohmyoh@ism.mech.tohoku.ac.jp, <sup>c</sup>muraoka@ipc.akita-u.ac.jp,

<sup>d</sup>ju@mech.nagoya-u.ac.jp, <sup>e</sup>sasagawa@cc.hirosaki-u.ac.jp

**Keywords:** Metallic Nanomaterials, Electromigration, Stress Migration, Nanocoils, Nanowelding

**Abstract.** Migration of atoms is presented to be utilized for fabrication of metallic micro/nanomaterials by controlling the phenomenon. Two kinds of migration phenomena are treated; one is electromigration and the other is stress migration. In addition to the formation of micro/nanomaterials, some achievements in enhancing their functions are demonstrated. One is a technique to fabricate nanocoils from the formed Cu nanowires. The others are techniques to weld or cut the micro/nanowires by using Joule heating. Finally, regarding evaluation of mechanical and electrical properties of the micro/nanomaterials, the concentrated-mass cantilever technique in atomic force acoustic microscopy and the four-point atomic force microscope technique are shown to be powerful tools, respectively.

### Introduction

Carbon nanotube, which is well-known nanomaterial, was discovered in 1991 [1] and it brought the innovation in nanoscience. Excellent properties of carbon nanotube such as mechanical, electrical, optical and thermal properties are expected to be used in many fields of applications. Metallic nanomaterials have also been found having excellent physical and chemical properties, and may be used as new functional elements, especially in NEMS or MEMS. So far, metallic nanomaterials are usually synthesized by chemical reaction [2,3].

In this paper, a new technology for fabricating the micro/nanomaterials (MNMs) by atomic diffusion is presented [4-8], see Fig. 1. Two kinds of atomic diffusion are treated; one is a phenomenon caused by electron flow in high density and called electromigration (EM) and the other is stress migration (SM) which depends on a gradient of hydrostatic stress in a sample. The methods without depending on the chemical properties of materials are expected that any element diffused by the atomic diffusion can be selected to form MNMs. The use of passivated metallic lines with a slit and small holes at the anode end of the lines is insisted in the formation of MNMs based on EM, where atoms are discharged from the small hole and form a material. Also it is shown by treating Cu that oxide layer on the surface of a sample plays a key role in the formation of nanowire (NW) based on SM. Metallic nanocoil (NC) is successfully fabricated from the formed Cu NW by inducing residual strain [9]. Moreover, the cutting and welding of Pt NWs are realized by

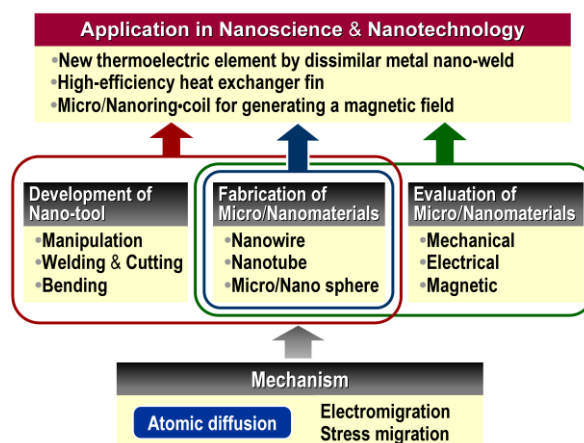


**Fig. 1** Study of metallic micro/nanomaterials.

Joule heating [10]. Finally, the special techniques based on atomic force microscopy (AFM) for evaluating the electrical [11] and mechanical properties of MNMs [12] are reported.

### Formation of Metallic Micro/Nanomaterials by Utilizing Electromigration

EM is a phenomenon that metallic atoms are transported by electron wind due to high density current in metals, and it is well-known as one of the key reasons of the metal line failure in electronic devices [13]. Recently, Saka *et al.* successfully fabricated the Al thin wires by utilizing EM [4,5]. Figure 2 illustrates the specimen for the fabrication [5]. When a direct current is applied to the specimen, electrons must flow inside the Al layer except for the slit portion at the anode end of line part, where TiN layer is bare. However Al atoms cannot pass the slit portion. Therefore, a lot of Al atoms will be accumulated near the anode end. The atoms are discharged from the pre-introduced hole and Al thin wire is formed; see Fig. 3(a). Also, it was demonstrated that the Al micro-spheres could be formed in the same specimen with the aid of the surface tension working on melted Al, see Fig. 3(b) [6]. It has been experimentally found that controlling EM enables us to selectively form thin Al wires and micro-spheres. Large micro-spheres are formed at high temperature of the atoms at the moment when the atoms complete to be discharged from the small holes at the anode end, wires at intermediate temperature, and small micro-spheres at low temperature [8]. However, in the actual situation, it is not an easy task to determine the temperature of atoms in advance because the temperature of atoms is affected by a number of factors such as the current density, substrate temperature and the geometry of the slit. The development of a new simulation code is helpful for discovering the effective parameters for MNM formation and it enables us to produce MNMs under the optimum conditions.

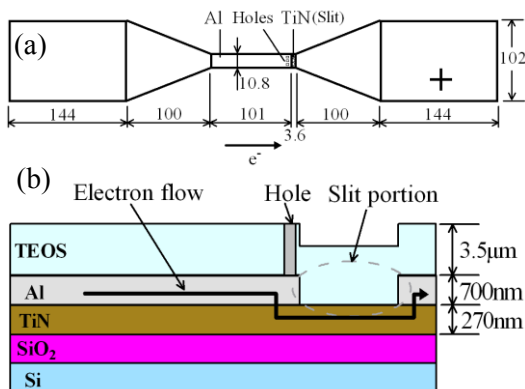


**Fig. 2** Example of passivated Al thin film specimen. (a) Top view. (b) Illustration of the electron flow in sectional view.

Sasagawa *et al.* have proposed an evaluation method of EM failure based on the numerical simulation [14], and the method has been improved for simulating the MNM formation. The simulation of MNM formation covers the concentration and overflow of the atoms and void initiation in the specimen, and the MNM formation is simulated by calculating the volume of the atoms overflowed from the specimen. Three combinations of the current density ( $j$ ) and substrate temperature ( $T_s$ ) shown in Table 1 were chosen as simulation conditions. The last column in Table 1 lists the predicted volume of MNM formed until specimen's failure defined based on the void initiation. It was shown that the volume is the largest under Condition 1 and smallest under Condition 3 due to difference of lifetime. The tendency of the change in volume obtained by the simulation was confirmed to be in good agreement with that for the corresponding experiments. We expect that the simulation-based approach will be a powerful tool for efficient fabrication of MNMs.

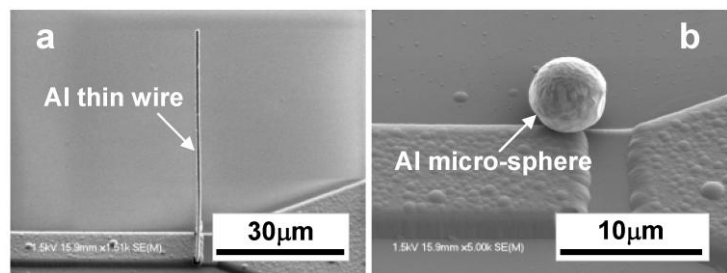


**Fig. 3** Example of MNMs. (a) Al thin wire. (b) Al micro-sphere.

**Table 1** Simulation conditions and results.

Condition	$j$ (MA/cm <sup>2</sup> )	$T_s$ (K)	Volume of MNMs (µm <sup>3</sup> )
1	2.4	653	9.5
2	2.6	613	7.5
3	2.8	553	6.2

Three combinations of the current density ( $j$ ) and substrate temperature ( $T_s$ ) shown in Table 1 were chosen as simulation conditions. The last column in Table 1 lists the predicted volume of MNM formed until specimen's failure defined based on the void initiation. It was shown that the volume is the largest under Condition 1 and smallest under Condition 3 due to difference of lifetime. The tendency of the change in volume obtained by the simulation was confirmed to be in good agreement with that for the corresponding experiments. We expect that the simulation-based approach will be a powerful tool for efficient fabrication of MNMs.

## Stress Migration

Stress migration is a phenomenon of atoms migration driven by the gradient of hydrostatic stress,  $\sigma$ . Atoms diffuse from a region of higher compressive stress towards that of lower stress. The atomic flux caused by stress migration,  $J_s$ , can be described as [15]

$$J_s = (C\Omega D_0)/(k_B T) \exp[-(Q - \Omega\sigma)/(k_B T)] \text{grad}\sigma, \quad (1)$$

where  $C$  is the atomic concentration,  $\Omega$  the atomic volume,  $k_B$  the Boltzmann's constant,  $T$  the absolute temperature,  $D_0$  the self-diffusion coefficient and  $Q$  the activation energy.

A 300 nm thick  $\text{SiO}_2$  layer was deposited on a Si (100) substrate. A 60 nm thick Ta layer was deposited on the  $\text{SiO}_2$  layer by sputtering. A 500 nm thick Cu film was then deposited on the Ta layer by an electron beam evaporation technique. This Cu/Ta/ $\text{SiO}_2$ /Si system is named Sample A. A ceramic heater positioned beneath the sample heated the sample uniformly under atmospheric conditions for 5 h at 613 K. A micrograph of the formulated Cu NWs obtained using a field emission scanning electron microscope (FE-SEM) is shown in Fig. 4(a).

When Sample A is heated, the Cu film is subjected to thermal stress because of the mismatch in thermal expansion coefficients between the metals, and the hydrostatic stress concentrations occur at the grain boundaries due to the anisotropy of the grains in the polycrystalline Cu films. The gradient of  $\sigma$  is the driving force for atomic diffusion and it is known that Cu atoms diffuse more easily on the surface than via grain boundaries. Therefore, atomic diffusion along the surface, especially the top surface of the Cu film, dominates the accumulation of Cu atoms. It is well-known that Cu is easily oxidized in the atmosphere, and an oxide layer ( $\text{Cu}_2\text{O}$ ) was observed on the surfaces of the samples. The  $\text{Cu}_2\text{O}$  layer plays a key role in the formation of Cu NWs [7]. If the compressive hydrostatic stress induced by the accumulation of Cu atoms at the interface between the oxide layer and the Cu film attains a critical value, then accumulated Cu atoms start to penetrate the oxide layer via any weak spots in the layer, after which Cu NWs are nucleated on its surface. The weak spots in the oxide layer form pathways through which Cu atoms can migrate externally due to the lower compressive stress that operates at the interface, and such weak spots may be located at the grain boundaries in the oxide layer.

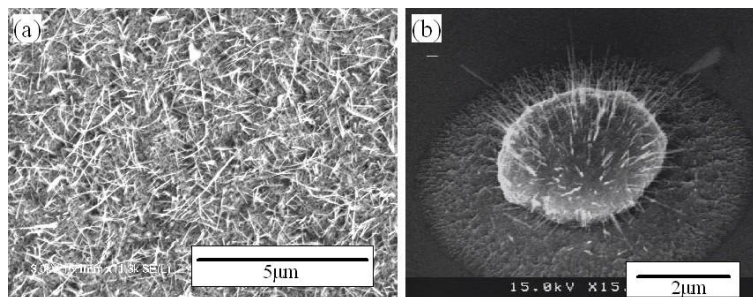


**Fig. 4** FE-SEM micrograph of Cu NWs formed on Sample A (a). FE-SEM micrograph of Cu NWs formed on a hillock on Sample B (b), where the hillock grew through a hole.

The growing positions of Cu NWs can be predetermined through controlling the positions of the weak spots [16]. On the basis of Sample A, a 600 nm thick Ta layer was sputtered on the top of the 450 nm thick Cu layer. Then holes with a diameter of 1  $\mu\text{m}$  were etched into the Ta and Cu layers by focused-ion-beam (FIB) technique. This Ta/Cu/Ta/ $\text{SiO}_2$ /Si system is named Sample B. The finite element analysis showed that lower compressive stress was generated at the Cu surface exposed by the holes, that is to say, the holes play the same role as the weak spots. Sample B was heated for 10 h at 613 K. It was observed through the FE-SEM micrograph that Cu hillocks grew through the holes and Cu NWs grew from the surfaces of the hillocks, as shown in Fig. 4(b).

### Fabrication of Nanocoils by Bending Straight Nanowires

Nanocoils (NCs) are candidates for nanoscale sensors and actuators, in addition to acting as mechanical springs. Self-assembly of NCs in the process of syntheses was reported for piezo-materials [17]. Carbon NCs were built up in the chemical vapor deposition assisted by spiral scanning of a FIB [18], and metal-coated carbon NCs were also fabricated for the improved conductivity. Conducting NCs are attractive to an application as small inductors. We developed an alternative technique for creating metal-coated NCs, which involves a process of bending a straight NW into a helix [9].

NWs are quite flexible but can hardly be deformed plastically. Instead, we used the residual strains induced by depositing overlayers on the surface of NWs. A deposited film generally possesses an internal intrinsic strain due to crystalline defects like crystal mismatch between a NW and an overlayer. The mismatched thermal strains also cause residual strains. A circumferentially biased thickness of an overlayer unbalances the residual strains and produces the bending deformation of a NW. We demonstrated metal-coated NCs, comprised of Cr-coated Cu NWs, with a coil diameter of about 300 to 500 nm. Figure 5 shows FE-SEM images of the Cr-coated Cu NCs, where straight Cu NWs yielded by SM [7] were bent by coating. Figure 5 (a) is the smallest metal-coated NC in the world. The Cr coating was performed with the electron-beam evaporation technique. The contribution to the bending process was mainly provided by the intrinsic strain. In addition, elastic anisotropy of the NWs coupled bending with a twist, contributes to the formation of helices.

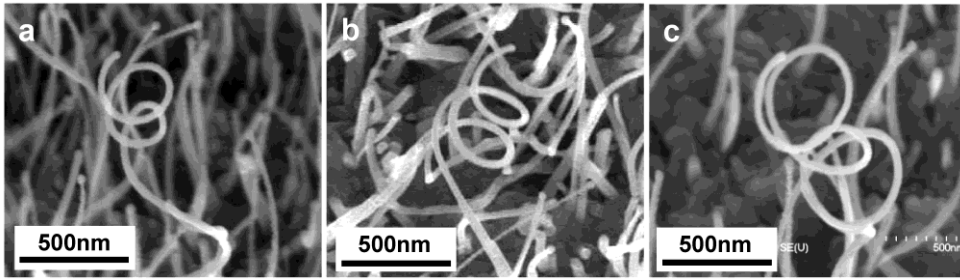


Fig. 5 Cr-coated Cu NCs, fabricated by bending straight Cu NWs.

### Cutting and Welding of Nanowires

The electro-thermal problem, where the current  $I$  flows through very-thin wire having the length of  $l$  and cross-sectional area of  $A$ , is considered. For simplicity, if we assume that no heat transfer from the surface of the wire to the atmosphere occurs, and the temperature at both the ends of the wire is constant at  $T_0$ , the solution of this heat conduction for steady-state temperature,  $T_1$ , is given by

$$T_1 = \frac{q}{2\kappa\rho c}(lx - x^2) + T_0, \quad (2)$$

where  $\rho$  is density,  $c$  specific heat,  $\kappa = K / (\rho c)$  and  $K$  heat conductivity, respectively. The  $x$ -axis is taken in the direction in the wire length and its origin locates at the one end of the wire. The quantity  $q = I^2 / (A^2 \sigma)$ , where  $\sigma$  is the electrical conductivity. Figure 6 shows the distributions of  $T_1$  against  $x$  for  $I = 4, 6$  and  $8$  mA in the case of the wire having the diameter of  $800$  nm and  $l = 200$   $\mu\text{m}$ . The material properties used in the calculation were:  $\sigma = 9.45 \times 10^6$  S/m,  $K = 72$  W/mK,  $\rho = 2.15 \times 10^4$  kg/m<sup>3</sup> and  $c = 134$  J/kg K, respectively. For all cases of  $I$ , the temperature takes its maximum value at the center of the wire, and the maximum value of  $T_1$  increases with increasing  $I$ . If we supply the current to the wire such that  $T_1$  at the center of the wire exceeds the melting point of the wire due to Joule heating and apply the force to shear the melting portion in the wire, the thin wire can be cut at the center of the wire.

The Pt NW having the diameter of  $800$  nm was examined in the cutting experiment. The cone-shaped Ag probes situated on the Cu electrode chips were used to locally supply the current to a

segment of the Pt NW. The faced Ag probes were contacted to the Pt NW with the separation distance of 200  $\mu\text{m}$ , and a small amount of force to separate the melting portion of the wire was applied by applying the small deflection of the NW with the Ag probes [Fig. 7(a)]. Immediately after the supply of current ( $I = 5.2 \text{ mA}$ ), the Pt NW was successfully cut in the middle of the probe separation [Fig. 7(b)].

The Pt NWs used in the welding experiments were the same as that used for the cutting experiment [10]. The Pt NWs were soldered on to the Cu electrode chips. Using the nano-manipulators, the tips of the Pt NWs were brought into contact with each other and a constant direct current of 4.8 mA was applied to the NW system. Figure 8(a) shows a FE-SEM micrograph of the weld, and it is clear that the NWs were welded together end to end in a continuous straight line. Note that the welding of dissimilar metals was also possible by the present techniques, and the Pt NW was successfully welded onto the Au wire having the diameter of 5  $\mu\text{m}$ , see Fig. 8(b).

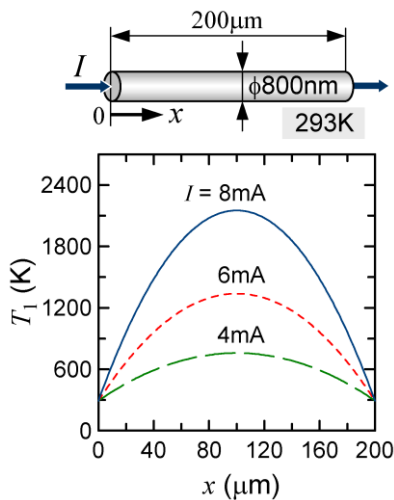


**Fig. 6** Distributions of  $T_1$  against  $x$  for the supplied current of 4, 6 and 8 mA. The one-dimensional electro-thermal problem was considered.

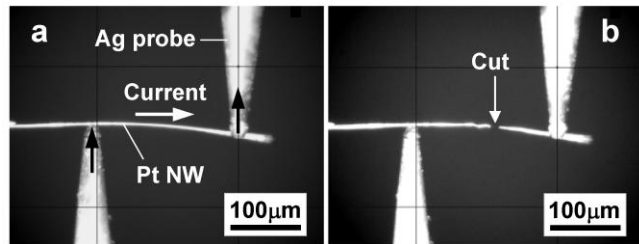


**Fig. 7** Digital microscope images of the cutting process. Without flowing current (a) and with current (b).

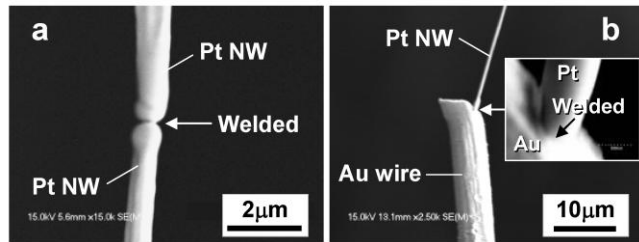


**Fig. 8** FE-SEM micrographs of the welds. (a) Straight welding of Pt NWs. (b) Pt NW was welded onto the Au wire.

### Quantitative Measurement of Local Conductivity of a Sub-micrometer Al Wire

Electrical conductivity of a 99.999% aluminum wire having a 400 nm width and a 200 nm thickness was measured using the four-point atomic force microscope (AFM) technique [11]. This technique is a combination of the principles of the four-point probe method and standard AFM. Figure 9 shows the SEM micrograph of the cantilever of the four-point AFM probe where the inset shows the enlarged tip of the probe. The spacing of the inner pair (electrodes 2, 3) is 300 nm and those of the outer pairs (electrodes 1, 2 & 3, 4) are 1.0  $\mu\text{m}$ .

Figures 10 and 11 show the topography image and typical current-voltage relationship of the Al wire, obtained by the four-point AFM probe, respectively. The method is capable of simultaneously measuring both surface topography and local conductivity. Experiments show that the microprobe is mechanically flexible and robust. The repeatability of conductivity measurements indicates that this four-point AFM probe could be used for fast *in situ* characterization of local electrical properties of nanocircuits and nanodevices.

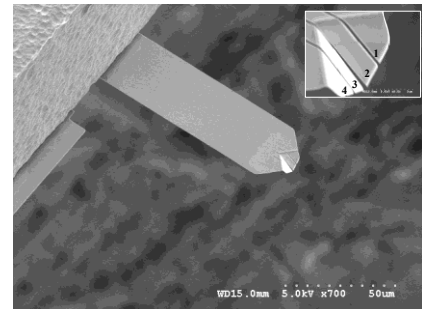


**Fig. 9** SEM micrograph of the cantilever of the four-point AFM probe and the enlarged tip (inset).

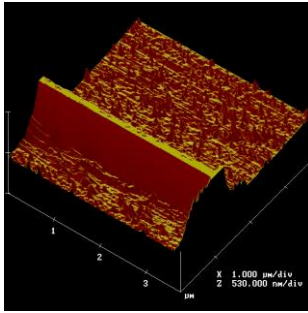


**Fig. 10** AFM topography image of the Al wire obtained by the four-point AFM probe.

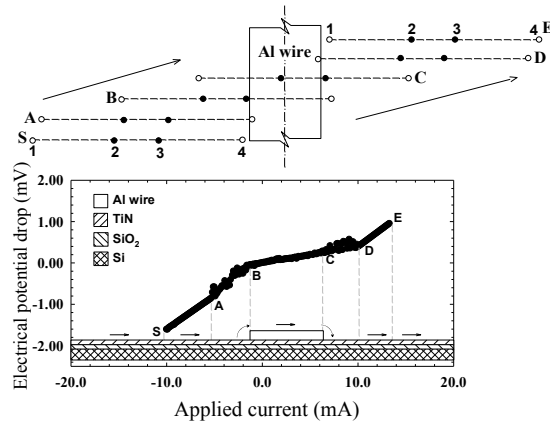


**Fig. 11** Typical current-voltage relationship of Al wire obtained by the four-point AFM probe. The AFM scanning direction was parallel to the Al wire's length.

### Determination of Elastic Properties by Concentrated-Mass Cantilever Technique

Atomic force acoustic microscopy (AFAM) [19] provides a possible technique for measuring the elastic modulus of nano-materials like NWs. In AFAM, the resonant frequency of a micro-cantilever equipped with a tip measures the contact stiffness between a tip and a sample. In the case of stiff samples like metals, usual AFAM exhibits low sensitivity. The proposed concentrated-mass (CM) cantilever offers a smart solution to the problem without trade-offs [12]. The dynamics of CM cantilevers is quite simple because the CM attached on the tip reduces the degree of vibration freedom. CM cantilevers behave as if they were one-freedom systems. The simple dynamics leads to an excellent agreement between experiment and theory.

Figure 12 shows examples of relationship between the resonant frequency of a CM cantilever and effective Young's modulus of a sample, where the theory (solid curves) agrees with the experiment (circles). The contact area of the tip sizes 10 nm or less. Therefore the curves are useful to determine the unknown modulus of NWs. Another type of CM cantilevers, having a rod-like CM, has two degrees of freedom and enables us to detect an effective shear modulus [20].

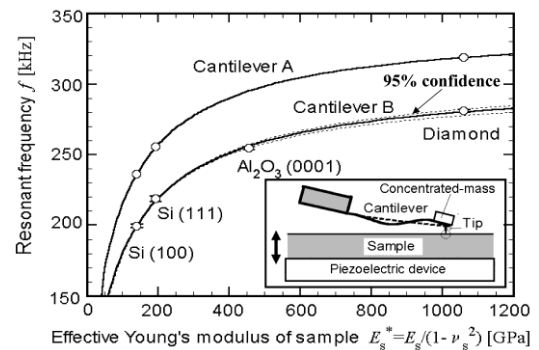


**Fig. 12** Resonant frequency of CM cantilevers (A and B) coupled with sample surface.

### Summary

Metallic micro/nanomaterials such as nanowires and micro-spheres have successfully been fabricated by utilizing migration of atoms, i.e., electromigration and stress migration. The techniques for bending, cutting and welding of nanowires are expected to be standard tools for application of micro/nanomaterials. Moreover, new techniques based on atomic force microscopy are powerful tools in evaluation of electrical and mechanical properties of micro/nanomaterials.

This work was supported by Grant-in-Aid for Scientific Research (S) 18106003.

**References**

- [1] S. Iijima: Nature Vol. 354 (1991), p. 56
- [2] Y. Xia, P. Yang, Y. Sun, Y. Wu, B. Mayers, B. Gates, Y. Yin, F. Kim, H.Q. Yan: Adv. Mater. Vol. 15 (2003), p. 353
- [3] J. Hu, T.W. Odom, C.M. Lieber: Acc. Chem. Res. Vol. 32 (1999), p. 435
- [4] M. Saka, R. Ueda: J. Mater. Res. Vol. 20 (2005), p. 2712
- [5] M. Saka and R. Nakanishi: Mater. Lett. Vol. 60 (2006), p. 2129
- [6] Y.X. Sun, H. Tohmyoh, M. Saka: J. Nanosci. Nanotechnol. Vol. 8 (2008), in press
- [7] M. Saka, F. Yamaya, H. Tohmyoh: Scripta Mater. Vol. 56 (2007), p. 1031
- [8] M. Saka, K. Kato, H. Tohmyoh, Y.X. Sun: J. Mater. Res. Vol. 23 (2008), p. 3122
- [9] M. Muraoka, N. Settsu, M. Saka: J. Nanosci. Nanotechnol. Vol. 8 (2008), p. 439
- [10] H. Tohmyoh, T. Imaizumi, H. Hayashi, M. Saka: Scripta Mater. Vol. 57 (2007), p. 953
- [11] B.-F. Ju, Y. Ju, M. Saka: J. Phys. D: Appl. Phys. Vol. 40 (1992), p.7467
- [12] M. Muraoka: Nanotechnology Vol. 16 (2005), p. 542
- [13] H. Abé, K. Sasagawa, M. Saka: Int. J. Fract. Vol. 138 (2006), p. 219
- [14] K. Sasagawa, M. Hasegawa, M. Saka, H. Abé: J. Appl. Phys. Vol. 91 (2002), p. 9005
- [15] C. Herring: J. Appl. Phys. Vol. 21 (1950), p. 437
- [16] N. Settsu, M. Saka, F. Yamaya: Strain Vol. 44 (2008), p.201
- [17] X. Y. Kong, Z. L. Wang: Nano Lett. Vol. 3 (2003), p. 1625
- [18] K. Nakamatsu, M. Nagase, J. Igaki, H. Namatsu, S. Matsui: J. Vac. Sci. Technol. Vol. B23 (2005), p. 2801
- [19] U. Rabe, K. Janser, W. Arnold: Rev. Sci. Instrum. Vol. 67 (1996), p. 3281
- [20] M. Muraoka: J. Phys.: Conf. Ser. Vol. 61 (2007), p. 836

# Transformation Plasticity - The Mechanism and Some Applications

Tatsuo Inoue

Department of Mechanical Systems Engineering, Fukuyama University,

Gakuen-cho 1, Fukuyama 729-0292I

inoue@fume.fukuyama-u.ac.jp

**Keywords:** Transformation plasticity, Unified transformation-thermoplasticity theory, metallo-thermo-mechanics, varying stress-temperature, Micromechanics.

**Abstract.** A phenomenological mechanism of transformation plasticity is discussed, in the first part of the paper, why the transformation plastic deformation takes place under a stress level even lower than the characteristic yield stress of the material: This is principally based on the difference in thermal expansion coefficient of mother and new phases. Some calculated data of induced stress and strain depending on applied stress are represented. Bearing in mind that it is also a kind of plastic strain, a unified plastic flow theory is derived by introducing the effect of progressing new phase into the yield function of stress, temperature and plasticity related parameters. Thus obtained strain rate reveals to include the transformation plastic part in addition to thermo-mechanical plastic components. Application of the theory is carried out to simulate some complicated cases of varying stress and temperature, and the results are compared with experimental data.

## Introduction

The transformation plasticity is known to contribute a drastic effect on the simulation of some practical engineering courses of thermo-mechanical processes [1-3], such as heat treatment, welding, casting and so on involving phase transformation of steels. Most constitutive laws for transformation plasticity, or TP [4-9] have been treated to be independent of ordinal thermo-plasticity.

Discussions on the mechanism why the transformation plasticity takes place in the course of phase transformation is made, in the first part of the paper, by using a simple model consisted of two bars of mother and new phase and how the rate of the strain is accelerated by applied stress to duplicate the temperature-elongation diagram. Considering that the mechanisms for both plastic strains are essentially with no difference from metallurgical viewpoint, the constitutive equation for transformation plastic strain rate is expected to be described in relation with plasticity theory [10-13]. This paper motivates to propose a mechanism for TP and to formulate unified constitutive equation of transformation and thermoplasticity by introducing the effect of increasing phase in mother phase.

Applications of the theory are made to numerical simulation of strain response under varying temperature and stress [14]. And, some discussion is attached for further consideration of practical simulation of the development of TP strain based on micromechanics.

## Mechanism of Transformation Plasticity

Fig. 1 depicts a model of temperature-elongation diagram for a fire resistant steel, FR-490A [15] during phase transformation. When the specimen is cooled down from austenite at 800°C within the cooling rate below lower critical rate, diffusion type phase, or pearlitic transformation occurs in between transformation start and end temperature of  $T_s=700$  and  $T_f=420$ °C.

Below the transformation start temperature  $T_s$ , a material element is assumed to be composed of mother and new phases connected parallelly as illustrated in Fig.2(a) [11-13]. Suppose that both phase elements are unreleased, element of mother phase, or austenite, shrinks much more than new phase under cooling operation since thermal expansion coefficient  $\alpha_m$  is larger than  $\alpha_n$  (Fig.2(b)),

which results in the progressive tensile stress in mother phase while compressive in new phase as shown in Fig.2(c). If the external tensile stress is applied like Fig.2(d) even lower than yield stress, total tensile stress in mother phase is enlarged sometimes to reach yield point and plastic deformation will take place. Volume fraction of new phase increases with decreasing temperature, this tensile stress in mother phase is expected to be enlarged before transformation is completed (See, Fig.2(e)). When applied external stress is in compressive, on the contrary, compressive plastic deformation may be induced in new phase. This is a simple mechanism of TP.

Denote the volume fractions of new and mother phases  $\xi_n$  and  $\xi_m$ . (In more general case to be discussed in the next section, the volume fraction of new phase will be denoted by  $\zeta_n$ .) When both elements are supposed to be connected parallelly like Fig.2(a), following relations hold when subjected to applied stress  $\sigma$  when considering the phase change dilatation  $\beta\xi_n$ ;

*Elastic-plastic constitutive equation;*

$$d\epsilon_m = \left( \frac{1}{E_m} + \frac{\delta_m}{H_m} \right) d\sigma_m + \alpha_m dT \quad \text{in mother phase} \quad (1a)$$

$$d\epsilon_n = \left( \frac{1}{E_n} + \frac{\delta_n}{H_n} \right) d\sigma_n + \alpha_n dT + \beta d\xi \quad \text{in new phase,} \quad (1b)$$

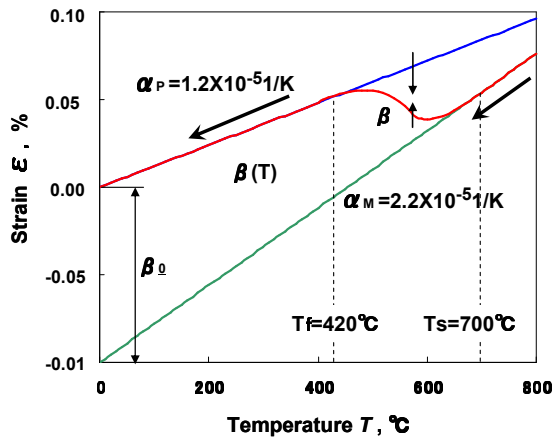


Fig.1 Temperature-elongation diagram

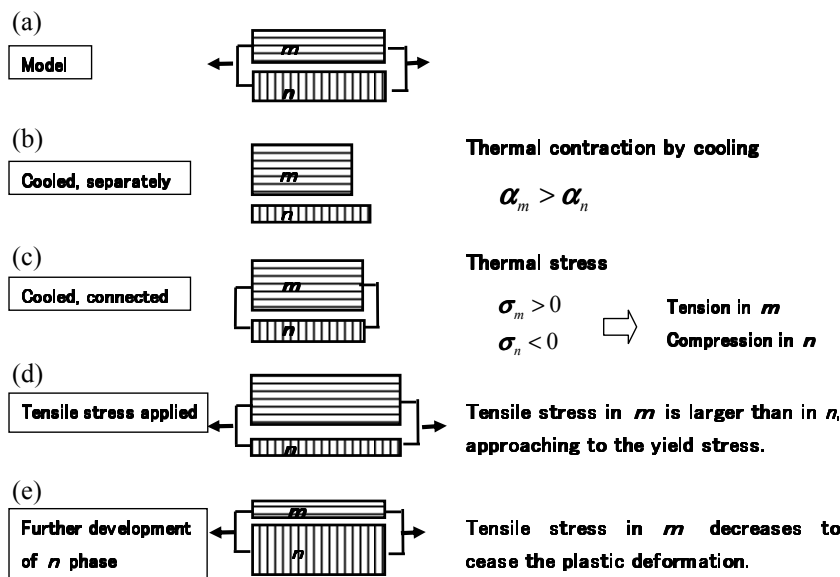


Fig.2 A model for transformation plasticity.

with  $\delta_m$  and  $\delta_n$  representing yield condition

$$\delta_m = \begin{cases} 1, & \text{if } \sigma_m \geq \sigma_{ms} \\ 0, & \text{if } \sigma_m < \sigma_{ms} \end{cases}, \delta_n = \begin{cases} 1, & \text{if } \sigma_n \geq \sigma_{ns} \\ 0, & \text{if } \sigma_n < \sigma_{ns} \end{cases} \quad (2)$$

where  $\sigma_{ms}$  and  $\sigma_{ns}$  are respectively yield stress of mother and new phase, being function of temperature determined by the database MATEQ, organized by our group, JSMS [16].

*Stress equilibrium condition;*

$$\sigma = \sigma_m \xi_m + \sigma_n \xi_n \quad \text{or} \quad d\sigma = d\sigma_m(1-\xi) + d\sigma_n \xi - \sigma_m d\xi + \sigma_n d\xi \quad \text{in incremental form}$$

with  $\xi_m + \xi_n = 1$ , or  $\xi_n \equiv \xi$  and  $\xi_m \equiv 1 - \xi$ , (3)

*Compatibility condition;*

$$\epsilon_m = \epsilon_n \quad \text{or} \quad d\epsilon_m = d\epsilon_n \quad (4)$$

Here,  $\sigma$ ,  $\epsilon$ ,  $E$ ,  $H$  and  $\alpha$  with suffix  $m$  or  $n$  denote the stress, strain, Young' modulus, plastic hardening modulus and linear expansion coefficient for mother and new phase,  $\beta$  is the expansion coefficient due to phase change, and  $T$  and  $T_s$  respectively stand for varying temperature and transformation start temperature.

The kinetics of pearlite transformation is assumed to be controlled by a function of temperature in the form,

$$\xi(T) = 1 - \exp\left[-\bar{k}(T - T_s)^{\bar{n}}\right], \quad \text{with} \quad \bar{k} = 2 \times 10^{-6}, \quad \bar{n} = 2.85, \quad T_s = 700 \quad , \quad (5)$$

by modifying the Johnson-Mehl formula with time  $\tau$ ,

$$\xi(\tau) = 1 - \exp\left[-k(\tau - \tau_s)^n\right] \quad . \quad (6)$$

Stress depending transformation start and finish temperature  $T_s, T_f$  are to be determined by use of Claudius-Clapeyron relation even in this case of solid-solid transformation. However, the data are quoted from the experiments by the authors [15].

Fig. 3 depicts the calculated result of variation of stresses induced in mother and new phases, and TP and total strains with respect to temperature as well as progress of new phase without externally applied stress.

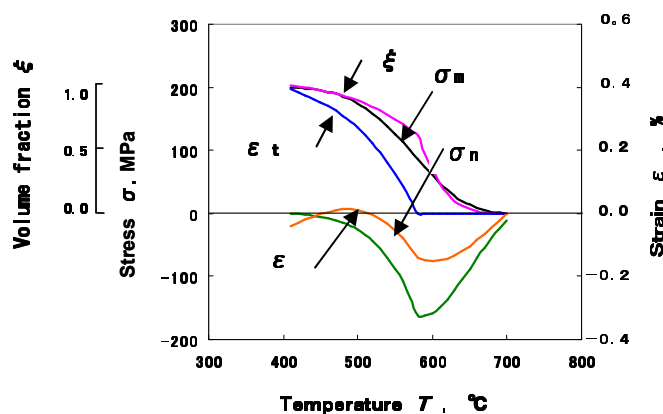


Fig.3 Variation of stresses in mother and new phase,  $\sigma_m$ ,  $\sigma_n$ , and TP and total strain  $\epsilon^{tp}$ ,  $\epsilon$  with progress of new phase  $\xi$ .

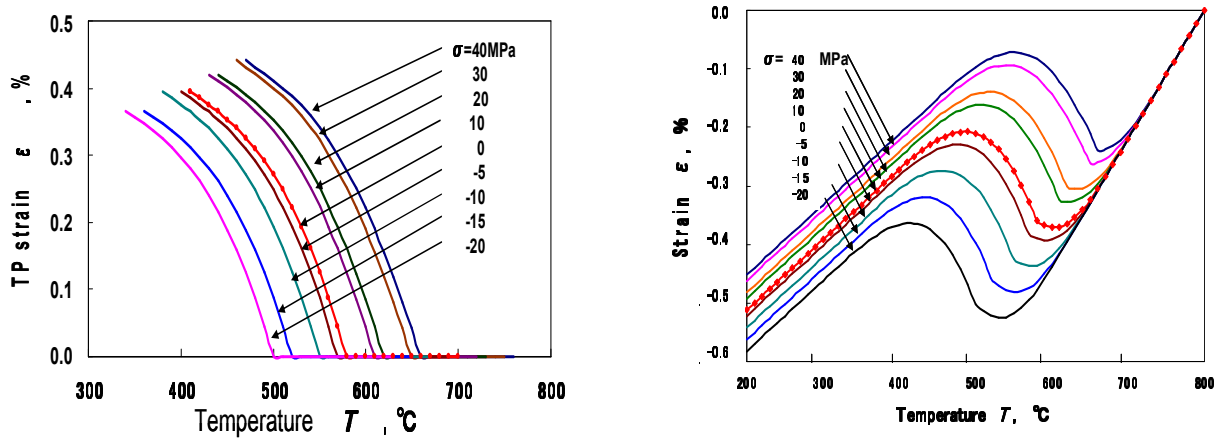
It is noted that plastic deformation occurs in the final stage during phase transformation even in the case without applied stress as seen in Fig.3, which will be discussed in latter section. Summarized data of temperature-total strain diagram depending of applied stress is represented in

Fig.4, which shows the quantitative correspondence with the experimental results. [14]. In the cooling process, phase transformation strain is generally increased since  $\alpha_m > \alpha_n$ , then the stresses in both phases tend to be positive in the final stage of phase change. Nevertheless, compressive stress in new phase is rather increased in the first stage, which would be possible to reach the compressive yield stress.

**The Unified Theory of Transformation-thermoplasticity**

In order to formulate a constitutive equation of a body under phase transformation, we assume that the material point focused is composed of  $N$  kinds of phases, which include all phases with the volume fraction  $\xi_I$  ( $I=1,2,3,\dots,N$ ) as is shown in Fig.6(a) and that the mechanical and thermophysical property  $\chi$  is represented by the *mixture law* [17] such that

$$\chi = \sum_{I=1}^N \xi_I \chi_I, \text{ with } \sum_{I=1}^N \xi_I = 1 \quad (7)$$



(a) TP strain (b) Total strain  
Fig.4 Applied stress dependence of TP and total strain.

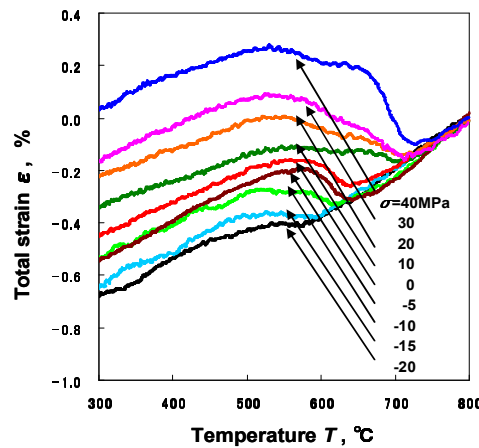


Fig.5 Experimental data of temperature-total strain diagram. .

Stress state related to the yielding of the  $I$ -th phase (say, mother phase) is assumed to be affected by other phases (new phase) with the volume fraction  $\xi_J$  ( $J=1,2,3,\dots,M$ ) as indicated in Fig.6(b). Then, the plasticity of the  $I$ -th phase is controlled by the yield function in the form,

$$F_I = F_I(\sigma_{ij}, T, \epsilon_{ij}^p, \kappa_I, \zeta_J), \quad (I = 1, 2, \dots, N ; J = 1, 2, \dots, M). \quad (8)$$

Here,  $\sigma_{ij}$ ,  $T$  and  $\kappa_I$  are respectively stand for uniform stress and temperature and plastic hardening parameter.

Applying the consistency relation and the normality law, we have the form of plastic strain rate of the  $I$ -th phase as

$$\dot{\epsilon}_{ij}^p = \Lambda_I \frac{\partial F_I}{\partial \sigma_{ij}} = \hat{G}_I \left[ \left( \frac{\partial F_I}{\partial \sigma_{kl}} \dot{\sigma}_{kl} + \frac{\partial F_I}{\partial T} \dot{T} \right) + \sum_{J=1}^M \frac{\partial F_I}{\partial \zeta_J} \dot{\zeta}_J \right] \frac{\partial F_I}{\partial \sigma_{ij}}, \quad (9)$$

with the hardening modulus  $\hat{G}_I$ .

The first term in Eq.(9) is the ordinal thermo-mechanical plastic strain rate in the  $I$ -th phase, which is superimposed mechanical and thermal parts. It is noted that the second term in Eq.(9) occurring in the  $I$ -th phase is originated from the progressing the new  $J$ -th phase  $\zeta_J$ , which is found to be so-called *transformation plastic strain rate*,

$$\dot{\epsilon}_{ij}^{tp} = \hat{G}_I \left( \sum_{J=1}^M \frac{\partial F_I}{\partial \zeta_J} \dot{\zeta}_J \right) \frac{\partial F_I}{\partial \sigma_{ij}}. \quad (10)$$

Adopting the mixture law, we finally have the global strain rate in the form

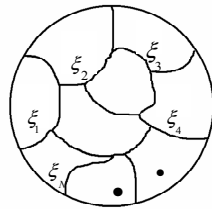
$$\dot{\epsilon}_{ij} = \dot{\epsilon}_{ij}^e + \dot{\epsilon}_{ij}^{th} + \dot{\epsilon}_{ij}^m + \dot{\epsilon}_{ij}^p. \quad (11)$$

Attention is focused on the unified plastic strain rate

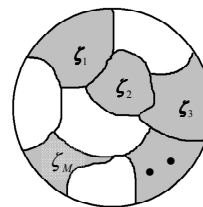
$$\dot{\epsilon}_{ij}^p = \sum_{I=1}^N \xi_I \dot{\epsilon}_{ij}^p = \sum_{I=1}^N \hat{G}_I \left[ \left( \frac{\partial F_I}{\partial \sigma_{kl}} \xi_I \dot{\sigma}_{kl} + \frac{\partial F_I}{\partial T} \xi_I \dot{T} \right) + \xi_I \left( \sum_{N=1}^N \frac{\partial F_I}{\partial \zeta_J} \dot{\zeta}_J \right) \right] \frac{\partial F_I}{\partial \sigma_{ij}}, \quad (12)$$

as the sum of thermo-mechanical and transformation plastic parts. The result indicates that both plastic strain rates related to thermo-mechanical and phase transformation effect is automatically derived from yield function in the form of Eq.(9) and that the Eq.(12) is the *unified plastic strain rate*. Now, consider a special case when uniaxial stress  $\sigma$  is applied. Then we have the transformation plastic strain rate as

$$\dot{\epsilon}^{tp} = \sum_{I=1}^N \frac{1}{H'_I} \left[ \sum_{J=1}^M \frac{H_{IJ}^\zeta \dot{\zeta}_J}{\bar{\sigma}_I} \xi_I \right] \sigma \quad (13)$$



(a) All phases



(b) Some phases associating plastic deformation.

Fig.6 Volume fraction of phases consisting a material point.

Here, hardening parameters are defined with the flow stress of the  $I$ -th phase  $\bar{\sigma}_I$ ,

$$H'_I = \frac{\partial \bar{\sigma}_I}{\partial \bar{\epsilon}_I^p} : \text{Strain hardening parameter of the } I\text{-th phase} \quad (14)$$

$$H_{IJ}^{\zeta} = \frac{\partial \bar{\sigma}_I}{\partial \zeta_J} \quad : \quad \text{Dependence of flow stress in the } I\text{-th phase on } J\text{-th phase} \quad (15)$$

And the constitutive equation for TP strain in case between the mother and new phase reads

$$\dot{\varepsilon}^{tp} = \frac{1}{H'_m} \left[ \left( \frac{H_{mm}^{\zeta} \dot{\zeta}_m}{\bar{\sigma}_m} + \frac{H_{mn}^{\zeta} \dot{\zeta}_n}{\bar{\sigma}_m} \right) \xi_m \right] \sigma + \frac{1}{H'_n} \left[ \left( \frac{H_{nm}^{\zeta} \dot{\zeta}_m}{\bar{\sigma}_n} + \frac{H_{nn}^{\zeta} \dot{\zeta}_n}{\bar{\sigma}_n} \right) \xi_n \right] \sigma, \quad (16)$$

with the flow stress  $\bar{\sigma}_m$ ,  $\bar{\sigma}_n$  of mother and new phase. Since the effect of structure on flow stress is possible;

$$H_{mn}^{\zeta} \neq 0, \quad \text{and} \quad H_{mm}^{\zeta} = H_{nn}^{\zeta} = H_{nn}^{\zeta} = 0. \quad (17)$$

And putting

$$\xi_m = 1 - \xi_n \equiv \xi, \quad \text{and} \quad \zeta_n \equiv \xi, \quad (18)$$

then we have

$$\dot{\varepsilon}^{tp} = \frac{1}{H'_m} \frac{H_{mn}^{\zeta} \dot{\xi}}{\bar{\sigma}_m} (1 - \xi) \sigma \equiv 3K (1 - \xi) \sigma. \quad (19)$$

This is the well known formula of Greenwood-Johnson for TP [4].

### Application to Strain Response for Complicated Stress and Temperature Variation

The theory developed is now applied to some cases under varying stress and temperature. Total strain in such cases of varying temperature is expressed as

$$\begin{aligned} \varepsilon(T) &= \varepsilon^e + \varepsilon^{th} + \varepsilon^m + \varepsilon^{tp} \\ &= \frac{\sigma}{E} + \int_{T_s}^T \left\{ \left[ \alpha_M (1 - \xi) + \alpha_N \xi \right] + \beta \frac{\partial \xi}{\partial T} \right\} dT + 3 \int_0^{\xi(T)} K (1 - \xi) \sigma d\xi \end{aligned} \quad (20)$$

The first case is to draw so-called temperature-elongation diagram. Fig. 7 depicts the experimental diagram during pearlite transformation of a Cr-Mo steel (SCM420) [18], which shows the strong stress dependence. Result of numerical calculation of Eq.(20) is plotted as temperature-elongation diagram is possible to be represented in Fig.7(a) for pearlite reaction, and also diagram for martensite transformation as shown in Fig.7(b). Here, Eqs. (5) and (6) are employed for diffusional and martensite transformation with the data of MATEQ [16], a material database accumulated by our group of Materials Database, JSMS. The coefficient of transformation plasticity ( $K = \sigma / \varepsilon^{tp} = 9 \times 10^{-5}$  1/MPa) for the steel is adopted by our experiment [18].

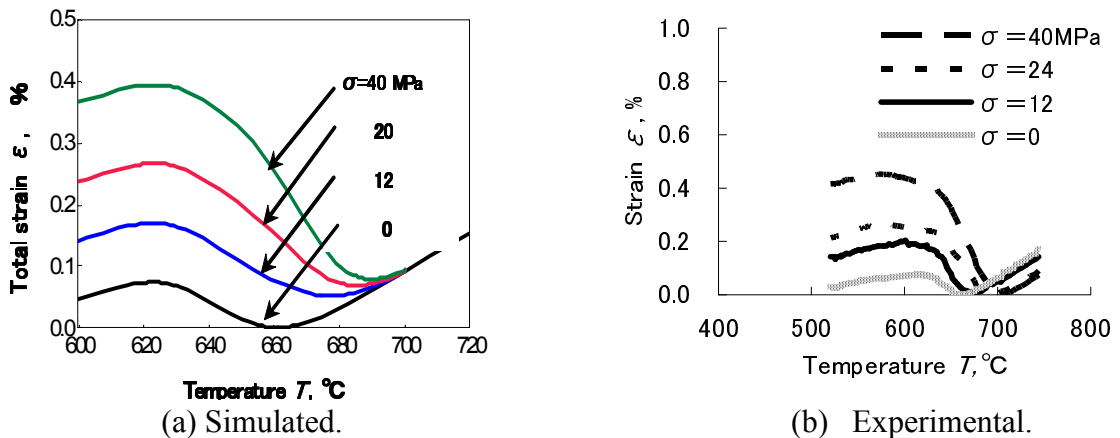


Fig.7 Temperature-elongation diagram – Cr-Mo steel.

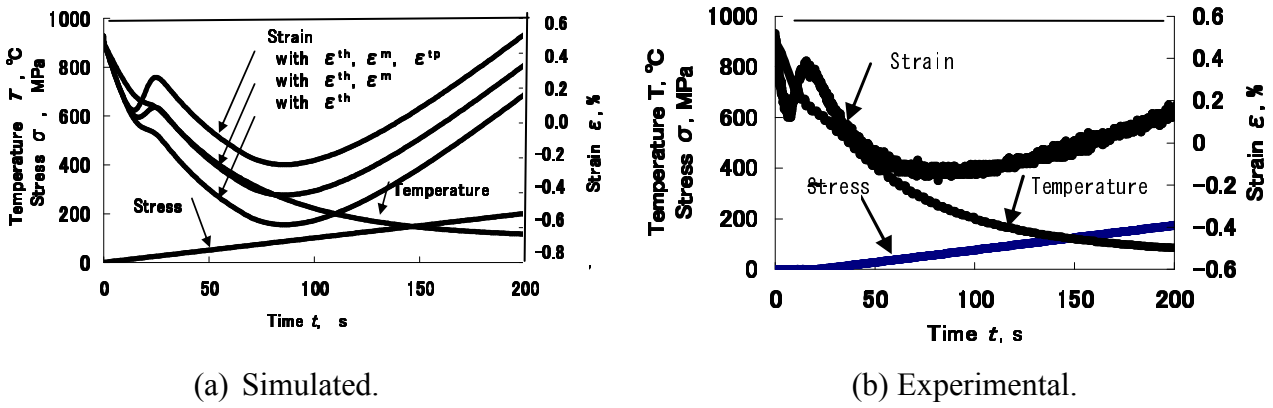


Fig.8 Strain response for varying stress and temperature.

The second example of application is related to fire extinguishment of structure made of a fire resistant steel (FR490A) cooled from 900°C with increasing stress [14]. Bottom line of strain variation in Fig.8 (a) represents the response considering only of thermal strain, and the middle is the one with phase transformation dilatation, while the upper result simulates the possible strain response including transformation plastic strain, which shows good agreement with the experimental data shown in Fig.8(b).

**Discussions from micromechanics viewpoint**

The simple two bar model discussed previously in Fig.2 gives a lot of interesting information on transformation plasticity. Nevertheless, some defects might be included if compared with real situation of transformation process.

Fig. 9 illustrates growing new phase in mother phase. Here, attention is to be focused that initiation sites of new phase is distributed in some spots in matrix in addition to the growth of new phase. The concept of extended volume fraction would be helpful in the later stage of phase transformation as indicated in the right figure.

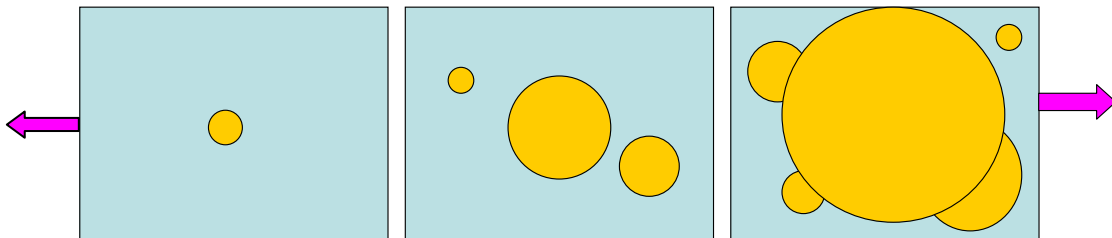


Fig.9 Schematic illustration of growing new phases in mother phase.

Detail simulation is now under operation by use of COSMAP, developed by Professor D.Y. Ju and the author [3] available to simulate metallo-thermo-mechanical processes. In the first step of consideration, progressing new phase from only one site is treated in the framework of elasticity.

So called *micromechanics* tells us that spherical inclusion of radius  $a$  with strain  $\epsilon^*_{ij} = \epsilon\delta_{ij}$  embedded in a infinite domain initially stress free region  $\Omega$  induces the strain [19];

$$\gamma_{mn}(x) = -\frac{\lambda\delta_{kl}\epsilon^*_{ii} + 2\mu\epsilon^*_{kl}}{8\pi\mu} \left( \delta_{km}\phi_{,ln} + \delta_{kn}\phi_{,lm} - \frac{\lambda + \mu}{\lambda + 2\mu} \psi_{,lkmn} \right) \tag{21}$$

where

$$\phi = \begin{cases} \frac{4}{3}\pi a^3/x, \\ 2\pi(a^2-x^2/3), \end{cases} \quad \psi = \begin{cases} \frac{4\pi}{3x}a^3\left(x^2+\frac{a^2}{5}\right), & \text{out of } \Omega \\ \frac{2\pi}{3}\left(\frac{3a^2}{2}+a^2x^2-\frac{x^4}{10}\right) & \text{in } \Omega \end{cases} \quad (22)$$

with

$$x = \sqrt{x_i x_i} \quad (23)$$

And stress is

$$\sigma_{pq}(x) = C_{pqmn} \gamma_{mn} = \frac{2\mu(1+\nu)}{3(1-\nu)} \varepsilon \begin{cases} a^3 \left( \frac{\delta_{pq}}{x^3} - \frac{3x_p x_q}{x^5} \right), & \text{out of } \Omega \\ -2\delta_{pq}, & \text{in } \Omega \end{cases} \quad (24)$$

or,

$$\sigma_{xx}(x) = \frac{2\mu(1+\nu)}{3(1-\nu)} \varepsilon \begin{cases} a^3 \left( \frac{1}{r^3} - \frac{3x^2}{r^5} \right), & \text{out of } \Omega \\ -2, & \text{in } \Omega \end{cases}$$

$$\sigma_{yy}(x) = \frac{2\mu(1+\nu)}{3(1-\nu)} \varepsilon \begin{cases} a^3 \left( \frac{1}{r^3} - \frac{3y^2}{r^5} \right), & \text{out of } \Omega \\ -2, & \text{in } \Omega \end{cases}$$

(25)

$$\sigma_{xy}(x) = \frac{2\mu(1+\nu)}{3(1-\nu)} \varepsilon \begin{cases} -a^3 \left( \frac{3xy}{r^5} \right), & \text{out of } \Omega \\ 0, & \text{in } \Omega \end{cases}$$

with

$$x = \sqrt{x^2 + y^2 + z^2} = r \quad (26)$$

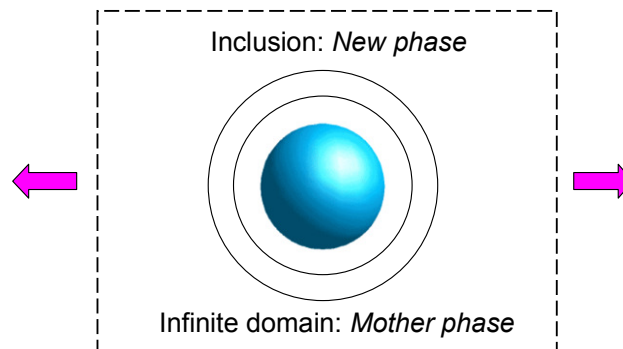


Fig.10 Schematic illustration of growing new phase in mother phase.

Here,  $a$  is the radius of inclusion,  $\lambda$ ,  $\mu$  and  $\nu$  stand for Lamé elastic constants.

This means that the inclusion gives stress decreasing in the manner of inversely proportion to the third power of radius from center out of the inclusion, while uniform compressive stress in  $\Omega$ .

Suppose that the radius of the inclusion representing the new pearlite phase increases with developing phase change in a manner

$$\varepsilon(T) = \beta \xi(T) \quad (27)$$

and

$$a(T) = A \beta \xi(T)^{1/3} \quad (A; \text{a parameter}) \quad (28)$$

Fig. 11 (a) and (b) represent the variation of stress distribution in radial and tangential direction  $\sigma_r$ ,  $\sigma_\theta$  along radius from center of the inclusion with progressing phase transformation with respect to temperature between  $T_s$  and  $T_f$ . The data shows that high tensile stress causes in tangential direction near the interface in the region out of  $\Omega$ , or in austenite structure, while compressive radial stress in other region. The equivalent stress  $\bar{\sigma}$  in the matrix near the interface is

$$\bar{\sigma} = |\sigma_r - \sigma_\theta| = \frac{3}{2} |\sigma_r| \quad (29)$$

will give a large value to cause the yielding, even if the stress is a little reduced due to stress concentration factor  $\alpha$  is less than unity when subjected to tensile stress.

Further elastic-plastic numerical calculation by FEM is expected in the finite domain considering the some site nucleation and the growth of new phase under varying temperature.

### Summary

A discussion on the mechanism from thermo-mechanical viewpoint is carried out, and the constitutive law is derived from unified thermomechanical-transformation plasticity theory. Application of the theory is made to some processes under varying temperature and stress, followed by the engineering simulation of quenching, which shows the importance of the transformation plasticity. Some discussions are attached on the mechanism of transformation plasticity, and the direction of future is appointed.

### Acknowledgement

The author is indebted to express his gratitude to IMS-Japan, NEDO and METI for their financial supports to this project. Thanks are also due to my students, T. Tanaka, K. Sato, A. Nishimura and H. Wakamatsu for their cooperation with experiments.

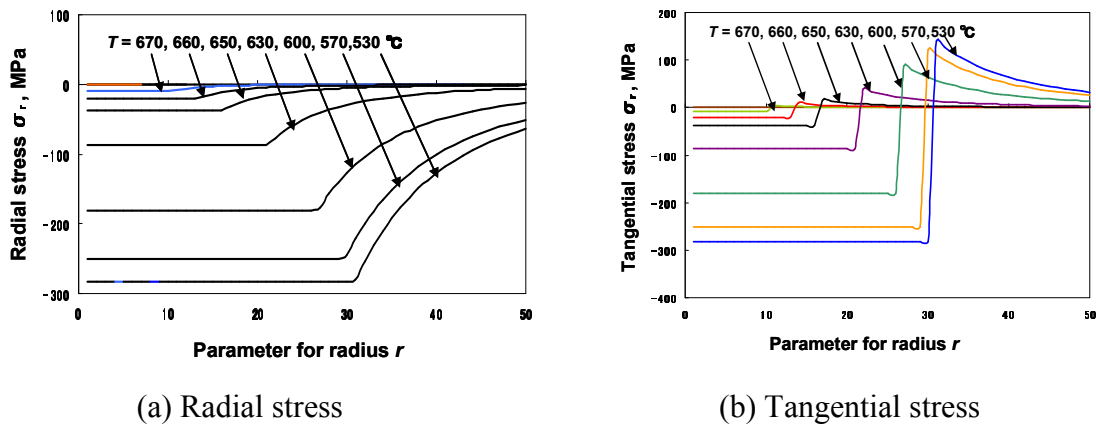


Fig.11 Progress of stresses with growing new phase.

### References

- [1] T. Inoue, T. Tanaka, D.Y. Ju and R. Mukai; Transformation Plasticity and the Effect on Quenching Process Simulation, Key Engineering Materials, Vol.345-346, 2007, pp.915-919.
- [2] Y. Watanabe, D.-Y. Ju, H. Shichino, K. Okamura, M. Narazaki, H. Kanamori, K. Ichitani and T. Inoue; Cooperative Research to Optimize Heat Treating Process Condition by Computer Based Technology, Solid State Phenomena, Vol. 118 (2006) pp. 349-354

- 
- [3] D.-Y. Ju and T. Inoue; On the material process simulation code COSMAP – Simulation examples and its experimental verification for heat treatment process, *Key Engineering Materials*, Vols. 345-346 (2007) pp. 955-958
- [4] G.W. Greenwood and R.H. Johnson; The deformation of metals under small stresses during phase transformations, *Proc. Roy. Soc.*, Vol. 283A, 1965, pp.403-422.
- [5] C.L Magee; *The Nucleation of Martensite*, Ch.3, ASM, 1968.
- [6] F.D. Fischer, G.E. Reisner, E. Werner, K. Tanaka and G. Gailletand; A new view on transformation induced plasticity, *Int J. plasticity*, Vol. 16, 2000, pp.723-740.
- [7] F. Barbe, R. Quer, L. Taleb and E.S. Cursi; FE determination of the effective TRIP during diffusive transformation in a volume with randomly positioned nuclei, *Proceedings of 1<sup>st</sup> Int. Conf. on Distortion Engineering*, Bremen, 2005, pp.149-148
- [8] J.B. Leblond; Mathematical modelling of transformation plasticity in steels, II Coupling with strian haredening phenomena, *Int J. Plasticity*, Vol.5, 1989, pp.1371-1391.
- [9] T. Otsuka, Y. Wakasu and T. Inoue; A simple identification of transformation plastic behavior and some data for heat treating materials, *Int. J. Mat. and Product Tech.*, Vol.4, 2005, pp.298-311.
- [10] T. Inoue; Unified transformation-thermoplasticity and the application (in Japanese), *J. Soc. Materials Science, Japan*, Vol.56, 2007, pp.354-358.
- [11] T. Inoue; On phenomenological mechanism of transformation plasticity and inelastic behavior of a steel subjected to varying temperature and stress --- Application of unified transformation-thermoplasticity Theory (in Japanese), *J. Soc. Materials Science, Japan*, Vol 57, 2008, pp.255-230.
- [12] T. Inoue; A phenomenological mechanism of transformation plasticity and the unified constitutive equation of transformation- thermo-mechanical plasticity, *Proceedings of Asia Pacific Conference on Computational Mechanics*, Kyoto, 2007, CD-published.
- [13] T. Inoue; Phenomenological mechanism of transformation plasticity and the constitutive law coupled with thermo-mechanical plasticity, *Advanced Materials Research*, Vol. 33-37, 2008, pp.1351-1358
- [14] T. Inoue, K. Sato and A. Nishimura; Elasto-plastic behavior of a fire resistant steel subjected to varying stress and temperature due to earthquake followed by fire, *Memoirs of Faculty of Engineering, Fukuyama University*, Vol.35 (2007), pp. 191-200.
- [15] H. Wakamatsu and T. Inoue; Identification of transformation plastic coefficient under tensile or compressive stress for some steels, *Preprint of 56<sup>th</sup> Annual Conference, Society of Materials Science, Japan, Kagoshima* (2008) pp.201-202.
- [16] T. Inoue and K. Okamura; Material database for simulation of metallo-thermo-mechanical fields, *Proceedings of 5th International Symposium on Quenching and Distortion Control*, ASM, 2000, pp.753-760.
- [17] R.M. Bowen; *Theory of Mixture*, A.C. Eringen, ed., *Continuum Physics* (Academic Press, New York, Vol. 3,1976, pp. 2-129.
- [18] T. Tanaka and T. Inoue; Identification of Transformation Plasticity Coefficient for Some Steels during Pearlite Transformation and the Dependence on Chemical Composition, (in Japanese), *J. Soc. Materials Science, Japan*, (in print)
- [19] J.D. Esherby; The determination of the elastic fields of an ellipsoidal inclusion, and related problems, *Proceedings of Loyal Society*, Vol. A241, (1957), pp.376-396.

## Nano-Size Surface Materials Stabilized by Weak Interaction

Ken-ichi Tanaka<sup>1)a</sup> and Xiaohong Jiang<sup>2)</sup>

<sup>1)</sup> Advanced Science Research Laboratory, Saitama Institute of Technology, 1690 Fusaiji, Fukaya, Saitama 369-0293, Japan

<sup>2)</sup> Key Laboratory for Special Functional Materials, Henan University, Kaifeng, 475001, China

<sup>a)</sup> ktanaka@sit.ac.jp

**Keywords:** Quasi-compound, (-Cu-O-) and (-Ag-O-) chain, Ag(110), Si(111)-7x7, Adsorption of C<sub>2</sub>H<sub>5</sub>OH, Surface migration, nano-dot of metals, Honeycomb layer of Zn<sub>3</sub>, Quantum effect, Bad gap.

**Abstract.** Scanning tunneling microscopy (STM) proved the existence of quasi-compounds on solid surfaces. A typical example is (-Ag-O-) or (-Cu-O-) chains grown on Ag(110) or Cu(110) surface by exposing to O<sub>2</sub>. The (-Ag-O-) chains on a Ag(110) reacts with Cu atoms to form a new quasi-compound of (-Cu-O-) chains on the Ag(110) surface. The (-Cu-O-) on the Ag(110) readily decomposes at ca. 570°K to form Cu<sub>6</sub> dots, and a reversible reaction of (Cu<sub>2</sub>)<sub>3</sub> + O<sub>2</sub>. ↔ (-Cu-O-) takes place by exposing to O<sub>2</sub>. Deposited Zn, Sn and Ag atoms on a Si(111)-7x7 surface stabilize by forming Zn<sub>3</sub>, Sn<sub>2</sub> and Sn, and Ag in a half unit cell. Layer-by-layer growth of Zn<sub>3</sub> clusters occurs in a half unit cell, which results in the growth of a semi-conductive honeycomb layer of Zn<sub>3</sub> clusters on the Si(111)-7x7 surface. By prohibiting hopping migration of Ag atoms on the Si(111)-7x7 surface by the adsorption of C<sub>2</sub>H<sub>5</sub>OH, nano-size Ag dots grow layer-by-layer in a limited mold spacing. The band gap of Ag-dots becomes narrower and narrower and becomes metallic at higher than 6 layers.

### 1) Introduction.

Atoms or molecules ordered or disordered array on the surface according to attractive or repulsive mutual interactions and adsorption induced local strain [1] as shown in Fig. 1.

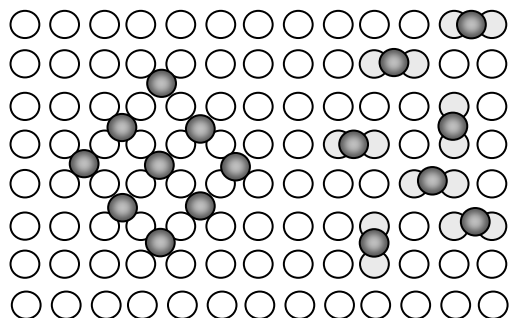


**Fig. 1.** Order or disorder array of adsorbed species and the local strain induced by the adsorption.

● Adsorbed atoms  
○ Strained surface atoms

Before the development of STM (scanning tunneling microscopy), however, we could not directly detect the local interaction as well as local strain in real space, especially weak interaction stabilizing nano-size materials on the surface.